ADVANCES IN ATMOSPHERIC SCIENCES, VOL. 39, NOVEMBER 2022, 1789–1799

• News & Views •

Typhoon Track, Intensity, and Structure: From Theory to Prediction※

Zhe-Min TAN*[1], Lili LEI[1], Yuqing WANG[2], Yinglong XU[3], and Yi ZHANG[1]

[1]*Key Laboratory of Mesoscale Severe Weather*, *Ministry of Education*, *and School of Atmospheric Sciences*, *Nanjing University*, *Nanjing* 210063, *China*

[2]*International Pacific Research Center*, *and Department of Atmospheric Sciences*, *School of Ocean and Earth Science and Technology*, *University of Hawaii at Manoa*, *Honolulu*, *Hawaii* 96822, *USA*

[3]*National Meteorological Center of CMA*, *Beijing* 100081, *China*

(Received 27 July 2022; revised 27 August 2022; accepted 31 August 2022)

ABSTRACT

To improve understanding of essential aspects that influence forecasting of tropical cyclones (TCs), the National Key Research and Development Program, Ministry of Science and Technology of the People's Republic of China conducted a five-year project titled "Key Dynamic and Thermodynamic Processes and Prediction for the Evolution of Typhoon Intensity and Structure" (KPPT). Through this project, new understandings of TC intensification, including outer rainband-driven secondary eyewall formation and the roles of boundary layer dynamics and vertical wind shear, and improvements to TC data assimilation with integrated algorithms and adaptive localizations are achieved. To promote a breakthrough in TC intensity and structure forecasting, a new paradigm for TC evolution dynamics (i.e., the correlations, interactions, and error propagation among the triangle of TC track, intensity, and structure) is proposed; and an era of dynamic-constrained, big-data driven, and strongly coupled data assimilation at the subkilometer scale and seamless prediction is expected.

Key words: typhoons, track, intensity, structure, theories, predictions

Citation: Tan, Z.-M., L. L. Lei, Y. Q. Wang, Y. L. Xu, and Y. Zhang, 2022: Typhoon track, intensity, and structure: from theory to prediction. *Adv. Atmos. Sci.*, **39**(11), 1789−1799, https://doi.org/10.1007/s00376-022-2212-1.

1. Introduction

The prediction of tropical cyclone (TC) track, intensity, and structure has been extremely challenging due to numerous factors. These factors include a lack of understanding of key dynamic and thermodynamic processes, large uncertainties from complex environments and internal dynamics, multi-scale interactions among different physical processes (e.g., radiation, planetary boundary layer, microphysics, etc.) and various geophysical components (e.g., ocean, land, and atmosphere), suboptimal assimilation of observations due to approximations and limitations of current analysis techniques, a large gap between the scales that observations and numerical models might represent or resolve, and limited representations of physical processes in numerical models.

Improving the understanding of physical processes within a wide range of scales involved in the development of TCs is a necessary and vital step towards better TC predictions. Pinpointing exact pathways of TC genesis remains one of the most mysterious and difficult challenges (e.g., Bister and Emanuel, 1997; Montgomery et al., 2006; Dunkerton et al., 2009; Emanuel, 2018), and a lack of understanding of those pathways prevents us from gaining a deeper understanding of TC climatology (e.g., Knutson et al., 2020; Sobel et al., 2021). After formation, exchanges between a TC and its underlying surface (e.g., ocean or land) determine the majority of energy source and dissipation in the system (Riehl, 1950; Kleinschmidt, 1951; Emanuel, 1986). Subsequent vertical transport and horizontal mixing of energy and momentum through turbulent flows are critical for the thermodynamic and dynamical structure in the boundary layer (e.g., Smith, 2003; Gopalakrishnan et al., 2013; Zhang et al., 2020), which further interacts with organized convection within the eyewall and rainbands (e.g., Schubert et al., 1999; Kossin and Schubert, 2001; Wang, 2009; Houze, 2010; Qiu and Tan, 2013). Feedbacks between

※ This paper is a contribution to the special topic on Key Dynamic and Thermodynamic Processes and Prediction of Typhoon (KPPT).

* Corresponding author: Zhe-Min TAN
Email: zmtan@nju.edu.cn

moist convection, radiation, and balanced and unbalanced flows in TC vortices govern the dynamics (e.g., Montgomery and Kallenbach, 1997; Kossin, 2002; Nolan and Montgomery, 2002; Nolan and Grasso, 2003; Dunion et al., 2014; Montgomery and Smith, 2014) and evolution of TC structure, leading to changes in TC track and intensity (e.g., Fovell et al., 2010; Bu et al., 2014; Tang and Zhang, 2016). These feedbacks are further complicated by interactions between the large-scale environment (e.g., vertical wind shear, outflow, and troughs) and the TC (e.g., Jones, 1995; Wang and Holland, 1996; Schecter et al., 2002; Riemer and Jones, 2010; Tang and Emanuel, 2010; Gu et al., 2015). Due to the multi-scale nature of TCs, any uncertainty in each of the above processes can propagate to other processes and finally manifest as larger uncertainties in general TC prediction (e.g., genesis, rapid intensification, precipitation, track), indicating the necessity of developing advanced techniques to minimize the original process uncertainties.

Many advanced techniques for TC forecasting, along with the usage of observations, have been proposed and investigated. Some commonly used techniques designed to improve TC initialization and produce better TC predictions include vortex bogusing, which incorporates artificial balanced TC-like vortices into the initial field (e.g., Leslie and Holland, 1995; Ueno, 1995; Kwon and Cheong, 2010), assimilation of synthetic observations (e.g., Zou and Xiao, 2000; Xiao et al., 2006; Davidson et al., 2014) and advisory observations (e.g., Torn, 2010; Kleist, 2011; Kunii, 2015), which provide estimates of TC position, intensity, and structure, and dynamical initialization, which inserts a spin-up vortex compatible with model physics into the model initial condition (e.g., Kurihara et al., 1995; van Nguyen and Chen, 2011; Liu and Tan, 2016). Advanced data assimilation approaches, from three-dimensional variational (3DVAR; e.g., Pu et al., 2009; Xiao et al., 2009) and four-dimensional variational (4DVAR; e.g., Zou and Xiao, 2000; Pu and Braun, 2001) methods to ensemble Kalman filters (EnKFs; e.g., Aksoy et al., 2013; Zhang et al., 2016), and to hybrid ensemble-variational methods (e.g., Lu and Wang, 2019; Wu et al., 2019), have been intensively examined for the purposes of data assimilation and TC forecasts. Various types of observations, including dropwindsonde observations (e.g., Wu et al., 2007; Weissmann et al., 2011), airborne Doppler radar data (e.g., Zhang et al., 2009; Dong and Xue, 2013; Aksoy et al., 2022), and satellite radiance observations (e.g., Honda et al., 2018; Zhu et al., 2019; Moradi et al., 2020), have been assimilated to help better resolve TC environments structures.

To further improve understanding of the essential aspects of TC forecasting, the National Key Research and Development Program, Ministry of Science and Technology of the People's Republic of China started the "Key Dynamic and Thermodynamic Processes and Prediction for the Evolution of Typhoon Intensity and Structure" project (KPPT), which spans the years 2018–22. The project focuses on the dynamics, physics, data assimilation, and prediction of typhoons. Research topics include dynamic and thermodynamic processes during TC evolution, predictability of TC track, intensity, and structure, key physical processes and parameterization schemes for the numerical modeling system, multi-scale ensemble-based data assimilation, effective usage of advanced observations like satellite radiances, and forecasting techniques for TC track, intensity, and structure. The project findings related to the evolutions of TC intensity and structure are summarized from two main perspectives: typhoon dynamics and associated environmental factors, and data assimilation and prediction for typhoons.

2. Typhoon dynamics and environmental influences

2.1. *Climate influences*

The recent global warming hiatus has contributed to the increased occurrence of intense TCs since 1998 along the coastal regions of East Asia (Zhao et al., 2018). Accumulated and averaged power dissipation indexes after TC landfalls over mainland China showed significant increasing trends during 1980–2018 as a result of increasing mean duration of TCs over land and increasing TC intensity at landfall (Liu et al., 2020). During 1980–2017, total annual TC precipitation exhibited an increasing trend in southeastern China due to an increase in annual TC precipitation frequency and precipitation intensity per TC; but annual TC precipitation exhibited a decreasing trend in southern China due to a reduced annual TC precipitation frequency (Liu and Wang, 2020). In the summer following a positive phase of the leading principal mode of the interannual variability in the Indo-Pacific warm pool (IPWP) Hadley circulation, there is increased TC genesis over the western North Pacific (WNP); the persistent impact of the leading principal mode until the summer is led by a positive wind–sea surface temperature (SST)–precipitation feedback (Guo and Tan, 2018a). Different types of El Niño–Southern Oscillation (ENSO) events can have different influences on rapid intensification (RI) of TCs over the WNP (Guo and Tan, 2018b, 2021). During short-duration El Niño events, the mean RI occurrence position of a WNP TC migrates westward by about 8.0° longitude. During La Niña events, the mean RI occurrence position during peak TC season shifts northward by about 2° latitude, while during eastern Pacific El Niño and La Niña events, the mean RI occurrence positions during late TC season shift westward by about 10° and 14° in longitude, respectively.

2.2. *Vertical wind shear*

Under environmental vertical wind shear (VWS), thermodynamic processes can help saturate the TC inner core before RI onset through an increase in the column-integrated moist static energy, highlighting the impact of vortex structure on TC

intensification (Chen et al., 2019). The outer-core convective-scale updrafts are weighted in favor of downshear formation, and the increase in the magnitude of VWS leads to more short-lived updrafts and decreased height of strong vertical velocities within convective bursts (Li and Fang, 2018). A downshear–upshear contrast in outer-core conditional instability occurs in weakly sheared TCs, while an enhanced downshear-left–downshear-right difference exists in strongly sheared TCs, which helps to maintain azimuthally asymmetric convective activity in the outer core of TCs (Li and Dai, 2020). TCs weaken rapidly for a relatively long period in upper-layer VWS, while they weaken initially but experience a quasi-periodic intensity oscillation in lower-layer VWS (Fu et al., 2019). Upper-layer VWS favors a better-organized stratiform sector in the outer rainbands compared to low-layer VWS, since the former produces a deeper asymmetric inflow layer in the outer rainband stratiform sector with more significant lower-level inflow and tangential jets (Gao et al., 2020). The balanced dynamics in response to the height-dependent vortex tilt determines the kinematic and thermodynamic structure of TCs embedded in a clockwise (CW) or counterclockwise (CC) directional shear flow (Gu et al., 2018, 2019). The height-dependent vortex tilt controls TC structural differences in CW and CC hodographs during the initial stage of development. The differences in the overall vortex tilt between CW and CC hodographs are amplified by a feedback from convective heating and result in higher intensification rates for TCs in CW hodographs than those in CC hodographs.

2.3. *Radiation, SST, and land–sea contrast*

Interactive radiation can facilitate TC genesis by accelerating the development of the midlevel vortex through a strong horizontal longwave radiative warming anomaly in the vortex region (Yang and Tan, 2020). Diurnal radiation has impacts on TC intensification through interactive processes in the boundary layer, including convection and radiation (Tang et al., 2019b).

SST played an essential role in the pre-landfall RI of Typhoon Mujigae (2015) by contributing to the formation of a strong/compact inner core with high precipitation symmetry (Chen et al., 2018). Similarly, the typhoon-induced warm coastal SST anomalies partly contributed to the pre-landfall RI of Typhoon Hato (2017) and slowed its weakening at and shortly after its landfall (Zhang et al., 2019). The TC superintensity decreases with increasing SST, which is dominated by the increased convective activity in the TC outer region for the SST-independent atmospheric initial condition or the increase in theoretical maximum potential intensity for the SST-dependent atmospheric initial condition (Li et al., 2020b). When an intense TC moves across a region with a sharp decrease in SST and into a region with large VWS and dry conditions in the upshear-left quadrant, the TC often experiences rapid weakening (Fei et al., 2020).

A distinct land–sea contrast in the diurnal variation of TC precipitation is found, with peak precipitation over land occurring in the afternoon and peak precipitation over the sea occurring in the early morning (Tang et al., 2019a). For Typhoon Longwang (2005), which produced catastrophic rainfall in Fujian Province of China, the terrain and landmass near Fujian greatly affected the structure and propagation of the TC rainbands (Li et al., 2020c). When Typhoon Megi (2010) crossed Luzon Island and entered the South China Sea, the landmass of Luzon Island contributed to the breakdown of the original eyewall and the formation of the new eyewall (Wang and Wang, 2021).

2.4. *TC structure*

Secondary eyewall formation (SEF) is regarded as a top-down process and is mainly triggered by axisymmetric and asymmetric dynamics (Wang et al., 2019a). TC tangential wind experiences outward expansion in response to diabatic heating in the outer rainband and inflow in the mid- to lower troposphere; the outer rainband is then intensified and rapidly axisymmetrized, and continuous inward propagation of perturbation wind and the rainband lead to SEF. The dynamics of SEF shows that the unbalanced boundary layer process driven by outer rainbands is essential for the canonical SEF, whose developments are governed by two different pathways, a wind-maximum formation pathway and a convective-ring formation pathway (Wang and Tan, 2020). Prior to the SEF, a double warm-core structure centered in the middle and upper troposphere occurs in the eye region; during the SEF, the double warm core structure rapidly strengthens, and the secondary off-center warm ring merges with the upper-level warm core to form a single warm core as the secondary eyewall intensifies and contracts and the primary eyewall weakens and dissipates (Wang et al., 2019b).

The TC fullness, as a new concept describing the maturity of TC structure, is positively correlated with TC intensity, and flight-level TC fullness increases more rapidly than near-surface TC fullness (Chen and Li, 2021). For strong typhoons and typhoons experiencing RI, there is greater overshooting top density (OTD, a proxy for deep convection with an intense updraft penetrating the tropopause) and greater diurnal variation of OTD (Sun et al., 2021). The low-level cold pool under the TC eyewall results from the evaporation of eyewall rainfall and acts as a barrier to boundary layer inflow, leading to enhanced convergence and vertical updraft at its outer edge, and hence promoting the formation of inner rainbands (Cai and Tang, 2019). Compared to normal TC rainbands, the secondary rainbands have distinctive features, such as a front-like structure, formation above the boundary layer, penetration of the lower portion of the mid-level inflow into the bottom of the convection tower, and concentration of the local maximum tangential wind in the updraft region (Xiao et al., 2019). The long-lasting spiral rainband of landfalling Typhoon Longwang (2005) originated from a previously existing wavenumber-2 vortex-Rossby wave and was maintained through the cold-pool dynamics and vertical wind shear-induced wavenumber-1 con-

vective forcing (Li et al., 2019).

For Typhoon Nepartak (2016), Wu and Fang (2019) showed that the midtropospheric vortex intensified once the deep convection strengthened and then weakened in the following shallow convection phase, and such processes recurred sequentially during the pregenesis of Nepartak (i.e., diurnal variations). Fang et al. (2019) further demonstrated that the most intense thermodynamic cycle in Hurricane Edouard (2014) was associated with the air rising within the hurricane eyewall, whose structure remained mostly steady during the early development but evolved rapidly as the storm intensified. Deepening of the thermodynamic cycle contributes to the increase of the mechanical work production and the Carnot efficiency during TC intensification. From theory to numerical simulations, Peng et al. (2018) divided TC intensification into two periods, phase I and phase II. During phase I, the TC intensifies while the angular momentum and saturation entropy surfaces evolve from nearly orthogonal to almost congruent; during phase II, the TC intensifies while the angular momentum and saturation entropy surfaces in the eyewall and outflow are congruent. The evolution of an axisymmetric TC during phase I is further investigated by Peng et al. (2019), who show that sporadic, deep convective annular rings play an important role in the axisymmetric TC evolution in phase I.

2.5. *Boundary layer processes*

Different from the common hypothesis for the role of the boundary layer in TC intensification, Li and Wang (2021a, b) demonstrate that TC intensification rate during the primary intensification stage is insensitive to surface drag coefficient. The effects of surface friction on the boundary-layer inflow and thus inner-core diabatic heating rate roughly offset the effect of surface friction on the TC dissipation rate. Meanwhile, TC intensification rate is sensitive to the initial TC structure, because the indirect heating effect of boundary layer dynamics strongly depends on vortex structure while the direct dissipation effect depends little on vortex structure. The positive upward advection of the supergradient wind from the boundary layer by eyewall updrafts is largely offset by the negative radial advection due to the outflow resulting from the outward agradient force (Li et al., 2020a). Thus, the upward advection of the supergradient wind component contributes little to the TC intensification rate but does contribute to the final TC intensity. Chen et al. (2021b) reveal that boundary layer recovery regulates the precipitation symmetrization and upshear deep convection, and further accounts for an earlier RI onset stage of the TC.

Chen et al. (2021c) compare a scale-aware planetary boundary layer (PBL) parameterization scheme to a non-scale-aware PBL scheme for TC intensification at subkilometer grid spacings and show that the scale-aware scheme tends to produce a stronger TC with a more compact inner core than the non-scale-aware scheme. Xu and Wang (2021) investigate fine-scale TC features with horizontal grid spacing reduced from 2 km to 55 m and demonstrate that TC intensity first increases and then decreases, but the opposite is true for TC inner core size. They suggest the use of sub-100-meter grid spacing to produce a more detailed and fine-scale structure of TC boundary-layer horizontal rolls and tornado-scale vortices.

3. Data assimilation and prediction

3.1. *Data assimilation algorithm*

An integrated hybrid ensemble Kalman filter (EnKF) that utilizes the framework of an EnKF to update both the ensemble mean and ensemble perturbations by the hybrid background error covariances is proposed by Lei et al. (2021), with the potential to improve small-scale features of a dynamic system. Increasing the assimilation frequency can help better extract information from dense temporal observations (e.g., radiance observations), but there is a trade-off between the assimilation frequency and imbalance that can be mitigated by a four-dimensional incremental analysis update (He et al., 2020). Multivariate ensemble sensitivity can accurately estimate the initial perturbations whose coherent structures lead to improved TC intensity forecast (Ren et al., 2019). For Typhoon Haiyan (2013), the initial dry dynamical differences play a more important role than the initial moist differences for the intensity changes, as revealed by the multivariate ensemble sensitivity.

3.2. *Radiance data assimilation*

Localization is essential for successful applications of EnKFs in high-dimensional geophysical systems, but it is not straightforward for radiance assimilation due to the lack of well-defined vertical locations. One strategy to overcome this is to implement model-space localization in EnKFs through a modulation approach; thus, no explicit vertical localization is necessary during the EnKF update (Lei et al., 2020b). Another strategy is adaptive localization, which uses sample correlations to provide an effective vertical localization function and associated localization parameters for each assimilated channel of every satellite platform (Lei et al., 2018). Furthermore, the adaptive localization method can provide adaptive localization parameters for different regions and times, which is beneficial for capturing the evolution of TCs, especially the onset of RI and subsequent intensity and structure changes (Wang et al., 2020). Although there is an increased need for computational resources, an ensemble with O(1000) members is sufficient to turn off the vertical localization and yields significant improvements compared to current, more computationally affordable ensembles with O(100) members (Lei et al., 2020b).

Measurements of cloud and microphysical properties are important for monitoring and assimilating the evolution of convective clouds. An algorithm is developed to determine the infrared (IR) cloud-top phase for advanced Himawari imager (AHI) measurements, and the product agrees with the Cloud–Aerosol Lidar with orthogonal polarization product and improves the presentations of ice-phase pixels over oceans and uncertain-phase pixels over land (Zhuge et al., 2021a). The AHI daytime cloud optical thickness and cloud-top particle effective radius are retrieved by the bispectral method (Zhuge et al., 2021b), and the retrievals are in good agreement with the Moderate Resolution Imaging Spectroradiometer cloud product (MOD06) product. Moreover, the simulations of AHI brightness temperature from three land surface emissivity datasets have negative biases relative to the observations made at night over China, with significant bias differences over grassland surface type (Zhuge et al., 2018), which suggests that spatially and temporally varying land surface emissivity datasets were used.

3.3. *Forecasts of TC track, intensity, and structure*

Systematic model errors of the geopotential height component that have similar features as the atmospheric semidiurnal tide contribute to the TC track forecast errors from the Global/Regional Assimilation and Prediction System (GRAPES), and by subtracting the model errors from the forecast equations, improved TC track forecasts are achieved (Zhou et al., 2018). To improve the predictive skill of ensemble forecasts for TCs, a method that estimates adaptive weights for members of an ensemble forecast is proposed (Lei et al., 2020a). The adaptive weights are estimated based on the fit of ensemble priors and posteriors to observations, by which the performances of ensemble forecasts are generally improved for TC track and intensity. Using an inverse method to estimate the true position error of TC track, Zhou and Toth (2020) demonstrate that the time limit of TC track predictability at the 181-nautical mile error level reached at day five in 2017 may be extended beyond six and eight days in 10 and 30 years' time, respectively, assuming an unabated pace of improvements to observing, modeling, and data assimilation.

To estimate TC intensity and wind radii from infrared (IR) imagery, a deep learning-based method augmented by prior knowledge of TCs (DeepTCNet) is introduced (Zhuo and Tan, 2021). With infused auxiliary physical information of TC fullness, DeepTCNet obtains improved TC intensity estimates; with simultaneous learning of TC wind radii and auxiliary TC intensity, DeepTCNet has improved estimates of wind radii. A seven-day TC intensity prediction scheme based on the logistic growth equation with a growth term and a decay term was developed for the WNP, and it has improved TC intensity forecasts and is better than the official intensity forecasts from the China Meteorological Administration (CMA), especially for TCs in the coastal regions of East Asia (Zhou et al., 2021). TC intensity forecasts in the WNP from five global ensemble prediction systems (EPSs) during 2015–19 show underestimation of TC intensity from ensemble mean forecasts and under-dispersion of probability forecasts (Xin et al., 2021). Although positive forecast skill was exhibited in 2018–19 at 120 h or later compared to climatology forecasts, no obvious improvement for the intensity change forecasts was shown during the five-year period, with abrupt intensity change remaining a big challenge.

The forecast performances of Typhoon Rammasun (2014) and Hato (2017) show that there exist defects in the subjective intensity forecast of the CMA, especially for lead times beyond 48 h. But forecasters can capture RI through local sea surface temperature and simulated warm core structure, which is beneficial for disaster reduction (Wang et al., 2019c). To bridge the gap between TC hazards and the associated socioeconomic impacts, "a potential risk index dataset for landfalling tropical cyclones over the Chinese mainland" (PRITC dataset V1.0) is produced (Chen et al., 2021a). The dataset includes TCs that made landfall from 1949–2018 and will be extended each year. It shows increased severity of TC impacts on the Chinese mainland, with the largest contribution coming from the increase in TC-induced precipitation.

4. Discussions and future challenges

Through the implementation of the "Key Dynamic and Thermodynamic Processes and Prediction for the Evolution of Typhoon Intensity and Structure" project, the knowledge of TC dynamic and thermodynamic processes, the understanding of environmental factors and climate variabilities influencing TC evolution, and data assimilation and forecast techniques for TC predictions, have been improved. However, there are yet to be any significant breakthroughs regarding TC intensity and structure forecasting. The common knowledge is that TC track is mainly influenced by large-scale circulations, while TC intensity is affected by processes across a wide range of scales. However, TC track, intensity, and structure should be considered coherently. TC intensity and structure and their evolutions are simultaneously influenced by the TC's dynamical and thermodynamic processes, including convection bursts, eyewall replacement cycles, outer and inner rainbands, etc. These structures and evolutions are also impacted by air–sea interactions (through boundary layer processes, SST responses, mesoscale vortices, etc.), complicated environments due to vertical wind shear and large-scale circulation, and the nonlinear interaction between the TC and its environment. Meanwhile, this nonlinear interaction in turn affects the TC track, whose change can result in substantial changes in TC intensity and structure. Thus, different from the common knowledge that separates factors influencing TC track and intensity, a new paradigm, a triangle of TC track, intensity, and structure, is proposed. As shown by Fig. 1, given a vortex position, TC intensity and structure are closely correlated; meanwhile, TC track has

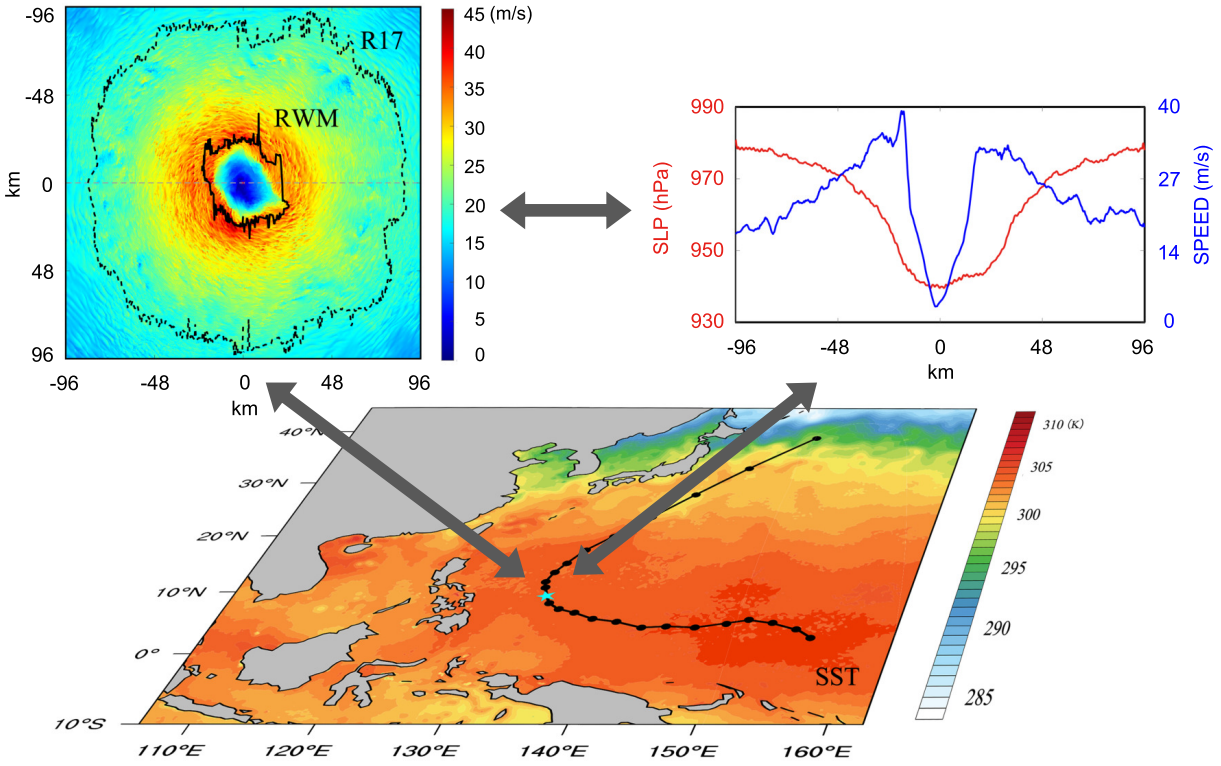

Fig. 1. Schematic diagram for the correlation triangle of TC track, intensity, and structure. The bottom panel shows SST (colored shading) and TC track (black line). The upper-left panel shows the 10-m wind speed from a simulated typhoon with 60-m horizontal spacing at the location of the star; the black solid and dashed lines denote the radius of maximum wind (RMW) and radius of gale-force wind (R17), respectively. The upper-right panel shows the sea level pressure and wind speed along the gray dashed line in the upper-left panel.

impacts on TC intensity and structure, and TC track is simultaneously influenced by TC intensity and structure. Therefore, one potential breakthrough for TC dynamics is to understand the correlations, interactions, and error propagations among the triangle of TC track, intensity, and structure.

From theory to practice, the predictability revealed by the error propagations among the triangle of TC track, intensity, and structure provides theoretical basis and guidance for future development of data assimilation and prediction of TCs. One consideration for data assimilation is the dynamic-constrained algorithm, from which dynamic-coherent analyses can be achieved and insights on observing strategies can be obtained. Another consideration for data assimilation is the challenge at fine resolutions (Fig. 1), due to the fast nonlinear error growth, severe model errors from poorly resolved physical processes, and etc. Given the continuous development of numerical models and observing networks, it is feasible to enter the era of big-data-driven data assimilation at subkilometer scales for TCs. However, the high spatial resolutions of numerical models and observations impose challenges for nonlinear data assimilation considering non-Gaussian error statistics and nonlinear error growth. Meanwhile, the high temporal resolution of numerical models and observations requires reformation for initialization and computing. Moreover, the triangle of TC track, intensity, and structure demands cross-scale data assimilation for TCs. Strongly coupled data assimilation, at least for the atmospheric and oceanic components, is required to sufficiently consider the important air–sea interactions and dynamic consistency.

Ensemble forecasts with probabilistic information are required for TC prediction. It is straightforward to launch ensemble forecasts for TCs from the ensemble initial conditions provided by dynamic-constrained and ensemble-based data assimilation with theoretical and practical knowledge of TC features embedded. Model errors result from under-represented physical processes; currently insufficient interactions among the physical processes need to be better represented, possibly from theoretical or data-driven views. Moreover, coupled data assimilation and prediction provide the possibility to enhance current TC forecasts into seamless TC predictions, which start from TC genesis and go throughout the whole TC lifecycle, with sufficient representations of TC intensity and structure evolution and the associated uncertainties. Nevertheless, great challenges remain for constructing unified models, cross-scale data assimilation, and ensemble predictions.

Acknowledgements. The authors would like to thank the anonymous reviewer for the insightful comments and suggestions. This work is supported by the National Key Research and Development Program of China (Grant Nos. 2017YFC1501600 and 2017YFC1501601).

REFERENCES

Aksoy, A., J. J. Cione, B. A. Dahl, and P. D. Reasor, 2022: Tropical cyclone data assimilation with coyote uncrewed aircraft system observations, very frequent cycling, and a new online quality control technique. *Mon. Wea. Rev.*, **150**, 797–820, https://doi.org/10.1175/MWR-D-21-0124.1.

Aksoy, A., S. D. Aberson, T. Vukicevic, K. J. Sellwood, S. Lorsolo, and X. J. Zhang, 2013: Assimilation of high-resolution tropical cyclone observations with an ensemble Kalman filter using NOAA/AOML/HRD's HEDAS: Evaluation of the 2008–11 vortex-scale analyses. *Mon. Wea. Rev.*, **141**, 1842–1865, https://doi.org/10.1175/MWR-D-12-00194.1.

Bister, M., and K. A. Emanuel, 1997: The genesis of Hurricane Guillermo: TEXMEX analyses and a modeling study. *Mon. Wea. Rev.*, **125**, 2662–2682, https://doi.org/10.1175/1520-0493(1997)125<2662:TGOHGT>2.0.CO;2.

Bu, Y. P., R. G. Fovell, and K. L. Corbosiero, 2014: Influence of cloud–radiative forcing on tropical cyclone structure. *J. Atmos. Sci.*, **71**, 1644–1662, https://doi.org/10.1175/JAS-D-13-0265.1.

Cai, Q. C., and X. D. Tang, 2019: Effect of the eyewall cold pool on the inner rainband of a tropical cyclone. *J. Geophys. Res.: Atmos.*, **124**, 1292–1306, https://doi.org/10.1029/2018JD029107.

Chen, P. Y., H. Yu, K. K. W. Cheung, J. J. Xin, and Y. Lu, 2021a: A potential risk index dataset for landfalling tropical cyclones over the Chinese mainland (PRITC dataset V1.0). *Adv. Atmos. Sci.*, **38**(10), 1791–1802, https://doi.org/10.1007/s00376-021-0365-y.

Chen, X. M., M. Xue, and J. Fang, 2018: Rapid intensification of Typhoon Mujigae (2015) under different sea surface temperatures: Structural changes leading to rapid intensification. *J. Atmos. Sci.*, **75**, 4313–4335, https://doi.org/10.1175/JAS-D-18-0017.1.

Chen, X. M., J. A. Zhang, and F. D. Marks, 2019: A thermodynamic pathway leading to rapid intensification of tropical cyclones in shear. *Geophys. Res. Lett.*, **46**, 9241–9251, https://doi.org/10.1029/2019GL083667.

Chen, X. M., J.-F. Gu, J. A. Zhang, F. D. Marks, R. F. Rogers, and J. J. Cione, 2021b: Boundary layer recovery and precipitation symmetrization preceding rapid intensification of tropical cyclones under shear. *J. Atmos. Sci.*, **78**, 1523–1544, https://doi.org/10.1175/JAS-D-20-0252.1.

Chen, X. M., M. Xue, B. W. Zhou, J. Fang, J. A. Zhang, and F. D. Marks, 2021c: Effect of scale-aware planetary boundary layer schemes on tropical cyclone intensification and structural changes in the gray zone. *Mon. Wea. Rev.*, **149**, 2079–2095, https://doi.org/10.1175/MWR-D-20-0297.1.

Chen, Z. H., and Q. Q. Li, 2021: Re-examining tropical cyclone fullness using aircraft reconnaissance data. *Adv. Atmos. Sci.*, **38**, 1596–1607, https://doi.org/10.1007/s00376-021-0282-0.

Davidson, N. E., and Coauthors, 2014: ACCESS-TC: Vortex specification, 4DVAR initialization, verification, and structure diagnostics. *Mon. Wea. Rev.*, **142**, 1265–1289, https://doi.org/10.1175/MWR-D-13-00062.1.

Dong, J. L., and M. Xue, 2013: Assimilation of radial velocity and reflectivity data from coastal WSR-88D radars using an ensemble Kalman filter for the analysis and forecast of landfalling hurricane *Ike* (2008). *Quart. J. Roy. Meteor. Soc.*, **139**, 467–487, https://doi.org/10.1002/qj.1970.

Dunion, J. P., C. D. Thorncroft, and C. S. Velden, 2014: The tropical cyclone diurnal cycle of mature hurricanes. *Mon. Wea. Rev.*, **142**, 3900–3919, https://doi.org/10.1175/MWR-D-13-00191.1.

Dunkerton, T. J., M. T. Montgomery, and Z. Wang, 2009: Tropical cyclogenesis in a tropical wave critical layer: Easterly waves. *Atmospheric Chemistry and Physics*, **9**, 5587–5646, https://doi.org/10.5194/acp-9-5587-2009.

Emanuel, K., 2018: 100 years of progress in tropical cyclone research. *Meteor. Monogr.*, **59**, 15.1–15.68, https://doi.org/10.1175/AMSMONOGRAPHS-D-18-0016.1.

Emanuel, K. A., 1986: An air-sea interaction theory for tropical cyclones. Part I: Steady-state maintenance. *J. Atmos. Sci.*, **43**, 585–605, https://doi.org/10.1175/1520-0469(1986)043<0585:AASITF>2.0.CO;2.

Fang, J., O. Pauluis, and F. Q. Zhang, 2019: The thermodynamic cycles and associated energetics of Hurricane Edouard (2014) during its intensification. *J. Atmos. Sci.*, **76**, 1769–1784, https://doi.org/10.1175/JAS-D-18-0221.1.

Fei, R., J. Xu, Y. Q. Wang, and C. Yang, 2020: Factors affecting the weakening rate of tropical cyclones over the Western North Pacific. *Mon. Wea. Rev.*, **148**, 3693–3712, https://doi.org/10.1175/MWR-D-19-0356.1.

Fovell, R. G., K. L. Corbosiero, A. Seifert, and K. N. Liou, 2010: Impact of cloud-radiative processes on hurricane track. *Geophys. Res. Lett.*, **37**, L07808, https://doi.org/10.1029/2010GL042691.

Fu, H., Y. Q. Wang, M. Riemer, and Q. Q. Li, 2019: Effect of unidirectional vertical wind shear on tropical cyclone intensity change—Lower-layer shear versus upper-layer shear. *J. Geophys. Res.: Atmos.*, **124**, 6265–6282, https://doi.org/10.1029/2019JD030586.

Gao, Q., Q. Q. Li, and Y. F. Dai, 2020: Characteristics of the outer rainband stratiform sector in numerically simulated tropical cyclones: Lower-layer shear versus upper-layer shear. *Adv. Atmos. Sci.*, **37**, 399–419, https://doi.org/10.1007/s00376-020-9202-y.

Gopalakrishnan, S. G., F. Marks Jr., J. A. Zhang, X. J. Zhang, J.-W. Bao, and V. Tallapragada, 2013: A study of the impacts of vertical diffusion on the structure and intensity of the tropical cyclones using the high-resolution HWRF system. *J. Atmos. Sci.*, **70**, 524–541, https://doi.org/10.1175/JAS-D-11-0340.1.

Gu, J.-F., Z.-M. Tan, and X. Qiu, 2015: Effects of vertical wind shear on inner-core thermodynamics of an idealized simulated tropical cyclone. *J. Atmos. Sci.*, **72**, 511–530, https://doi.org/10.1175/JAS-D-14-0050.1.

Gu, J.-F., Z.-M. Tan, and X. Qiu, 2018: The evolution of vortex tilt and vertical motion of tropical cyclones in directional shear flows. *J. Atmos. Sci.*, **75**, 3565–3578, https://doi.org/10.1175/JAS-D-18-0024.1.

Gu, J.-F., Z.-M. Tan, and X. Qiu, 2019: Intensification variability of tropical cyclones in directional shear flows: Vortex tilt-convection coupling. *J. Atmos. Sci.*, **76**, 1827–1844, https://doi.org/10.1175/JAS-D-18-0282.1.

Guo, Y.-P., and Z.-M. Tan, 2018a: Impacts of the boreal spring Indo-Pacific Warm Pool Hadley circulation on tropical cyclone activity

over the Western North Pacific. *J. Climate*, **31**, 1361–1375, https://doi.org/10.1175/JCLI-D-17-0422.1.

Guo, Y.-P., and Z.-M. Tan, 2018b: Westward migration of tropical cyclone rapid-intensification over the northwestern Pacific during short duration El Niño. *Nature Communication*, **9**, 1507, https://doi.org/10.1038/s41467-018-03945-y.

Guo, Y.-P., and Z.-M. Tan, 2021: Influence of different ENSO types on tropical cyclone rapid intensification over the western North Pacific. *J. Geophys. Res.: Atmos.*, **126**, e2020JD033059, https://doi.org/10.1029/2020JD033059.

He, H., L. L. Lei, J. S. Whitaker, and Z.-M. Tan, 2020: Impacts of assimilation frequency on Ensemble Kalman filter data assimilation and imbalances. *Journal of Advances in Modeling Earth Systems*, **12**, e2020MS002187, https://doi.org/10.1029/2020MS002187.

Honda, T., and Coauthors, 2018: Assimilating all-sky *Himawari-8* satellite infrared radiances: A case of Typhoon Soudelor (2015). *Mon. Wea. Rev.*, **146**, 213–229, https://doi.org/10.1175/MWR-D-16-0357.1.

Houze, R. A. Jr., 2010: Clouds in tropical cyclones. *Mon. Wea. Rev.*, **138**, 293–344, https://doi.org/10.1175/2009MWR2989.1.

Jones, S. C., 1995: The evolution of vortices in vertical shear. I: Initially barotropic vortices. *Quart. J. Roy. Meteor. Soc.*, **121**, 821–851, https://doi.org/10.1002/qj.49712152406.

Kleinschmidt, E. Jr., 1951: Grundlagen einer theorie der tropischen zyklonen. *Arch. Meteor. Geophys. Bioklimatol. Ser. A*, **4**, 53–72, https://doi.org/10.1007/BF02246793.

Kleist, D. T., 2011: Assimilation of tropical cyclone advisory minimum sea level pressure in the NCEP global data assimilation system. *Wea. Forecasting*, **26**, 1085–1091, https://doi.org/10.1175/WAF-D-11-00045.1.

Knutson, T., and Coauthors, 2020: Tropical cyclones and climate change assessment: Part II: Projected response to anthropogenic warming. *Bull. Amer. Meteor. Soc.*, **101**, E303–E322, https://doi.org/10.1175/BAMS-D-18-0194.1.

Kossin, J. P., 2002: Daily hurricane variability inferred from GOES infrared imagery. *Mon. Wea. Rev.*, **130**, 2260–2270, https://doi.org/10.1175/1520-0493(2002)130<2260:DHVIFG>2.0.CO;2.

Kossin, J. P., and W. H. Schubert, 2001: Mesovortices, polygonal flow patterns, and rapid pressure falls in hurricane-like vortices. *J. Atmos. Sci.*, **58**, 2196–2209, https://doi.org/10.1175/1520-0469(2001)058<2196:MPFPAR>2.0.CO;2.

Kunii, M., 2015: Assimilation of tropical cyclone track and wind radius data with an ensemble Kalman filter. *Wea. Forecasting*, **30**, 1050–1063, https://doi.org/10.1175/WAF-D-14-00088.1.

Kurihara, Y., M. A. Bender, R. E. Tuleya, and R. J. Ross, 1995: Improvements in the GFDL hurricane prediction system. *Mon. Wea. Rev.*, **123**, 2791–2801, https://doi.org/10.1175/1520-0493(1995)123<2791:IITGHP>2.0.CO;2.

Kwon, I. H., and H. B. Cheong, 2010: Tropical cyclone initialization with a spherical high-order filter and an idealized three-dimensional bogus vortex. *Mon. Wea. Rev.*, **138**, 1344–1367, https://doi.org/10.1175/2009MWR2943.1.

Lei, L. L., J. S. Whitaker, and C. Bishop, 2018: Improving assimilation of radiance observations by implementing model space localization in an ensemble Kalman filter. *Journal of Advances in Modeling Earth Systems*, **10**, 3221–3232, https://doi.org/10.1029/2018MS001468.

Lei, L. L., Y. J. X. Ge, Z.-M. Tan, and X. W. Bao, 2020a: An evaluation and improvement of tropical cyclone prediction in the western North Pacific basin from global ensemble forecasts. *Science China Earth Sciences*, **63**, 12–26, https://doi.org/10.1007/s11430-019-9480-8.

Lei, L. L., J. S. Whitaker, J. L. Anderson, and Z.-M. Tan, 2020b: Adaptive localization for satellite radiance observations in an ensemble Kalman filter. *Journal of Advances in Modeling Earth Systems*, **12**, e2019MS001693, https://doi.org/10.1029/2019MS001693.

Lei, L. L., Z. R. Wang, and Z.-M. Tan, 2021: Integrated hybrid data assimilation for an ensemble Kalman filter. *Mon. Wea. Rev.*, **149**, 4091–4105, https://doi.org/10.1175/MWR-D-21-0002.1.

Leslie, L. M., and G. J. Holland, 1995: On the bogussing of tropical cyclones in numerical models: A comparison of vortex profiles. *Meteorol. Atmos. Phys.*, **56**, 101–110, https://doi.org/10.1007/BF01022523.

Li, Q. Q., and Q. X. Fang, 2018: A numerical study of convective-scale structures in the outer cores of sheared tropical cyclones: 1. Updraft traits in different vertical wind shear magnitudes. *J. Geophys. Res.: Atmos.*, **123**, 12 097–12 116, https://doi.org/10.1029/2018JD029022.

Li, Q. Q., and Y. F. Dai, 2020: Revisiting azimuthally asymmetric moist instability in the outer core of sheared tropical cyclones. *Mon. Wea. Rev.*, **148**, 1297–1319, https://doi.org/10.1175/MWR-D-19-0004.1.

Li, T.-H., and Y. Q. Wang, 2021a: The role of boundary layer dynamics in tropical cyclone intensification. Part I: Sensitivity to surface drag coefficient. *J. Meteor. Soc. Japan. Ser. II*, **99**(2), 537–554, https://doi.org/10.2151/jmsj.2021-027.

Li, T.-H., and Y. Q. Wang, 2021b: The role of boundary layer dynamics in tropical cyclone intensification. Part II: Sensitivity to initial vortex structure. *J. Meteor. Soc. Japan. Ser. II*, **99**(2), 553–573, https://doi.org/10.2151/jmsj.2021-028.

Li, Y.-L., Y.-L. Lin, and Y. Q. Wang, 2019: A numerical study on the formation and maintenance of a long-lived rainband in Typhoon Longwang (2005). *J. Geophys. Res.: Atmos.*, **124**(19), 10 401–10 426, https://doi.org/10.1029/2019JD030600.

Li, Y.-L., Y. Q. Wang, and Y.-L. Lin, 2020a: How much does the upward advection of the supergradient component of boundary layer wind contribute to tropical cyclone intensification and maximum intensity? *J. Atmos. Sci.*, **77**(8), 2649–2664, https://doi.org/10.1175/JAS-D-19-0350.1.

Li, Y.-L., Y. Q. Wang, Y.-L. Lin, and R. Fei, 2020b: Dependence of superintensity of tropical cyclones on SST in axisymmetric numerical simulations. *Mon. Wea. Rev.*, **148**, 4767–4781, https://doi.org/10.1175/MWR-D-20-0141.1.

Li, Y.-L., Y. Q. Wang, Y.-L. Lin, R. Fei, and J.-Y. Gao, 2020c: Effects of terrain and landmass near Fujian Province of China on the structure and propagation of a long-lived rainband in Typhoon Longwang (2005): A numerical study. *J. Geophys. Res.: Atmos.*, **125**, e2020JD033393, https://doi.org/10.1029/2020JD033393.

Liu, H. Y., and Z. M. Tan, 2016: A dynamical initialization scheme for binary tropical cyclones. *Mon. Wea. Rev.*, **144**, 4787–4803, https://doi.org/10.1175/MWR-D-16-0176.1.

Liu, L., and Y. Q. Wang, 2020: Trends in landfalling tropical cyclone-induced precipitation over China. *J. Climate*, **33**(6), 2223–2235,

https://doi.org/10.1175/JCLI-D-19-0693.1.
Liu, L., Y. Q. Wang, R.-F. Zhan, J. Xu, and Y. H. Duan, 2020: Increasing destructive potential of landfalling tropical cyclones over China. *J. Climate*, **33**(9), 3731–3743, https://doi.org/10.1175/JCLI-D-19-0451.1.
Lu, X., and X. G. Wang, 2019: Improving Hurricane analyses and predictions with TCI, IFEX field campaign observations, and CIMSS AMVs using the advanced hybrid data assimilation system for HWRF. Part I: What is missing to capture the rapid intensification of Hurricane Patricia (2015) when HWRF is already Initialized with a More Realistic Analysis? *Mon. Wea. Rev.*, **147**, 1351–1373, https://doi.org/10.1175/MWR-D-18-0202.1.
Montgomery, M. T., and R. J. Kallenbach, 1997: A theory for vortex Rossby-waves and its application to spiral bands and intensity changes in hurricanes. *Quart. J. Roy. Meteor. Soc.*, **123**, 435–465, https://doi.org/10.1002/qj.49712353810.
Montgomery, M. T., and R. K. Smith, 2014: Paradigms for tropical cyclone intensification. *Australian Meteorological and Oceanographic Journal*, **64**, 37–66, https://doi.org/10.22499/2.6401.005.
Montgomery, M. T., M. E. Nicholls, T. A. Cram, and A. B. Saunders, 2006: A vortical hot tower route to tropical cyclogenesis. *J. Atmos. Sci.*, **63**, 355–386, https://doi.org/10.1175/JAS3604.1.
Moradi, I., K. F. Evans, W. McCarty, M. Cordero-Fuentes, R. Gelaro, and R. A. Black, 2020: Assimilation of satellite microwave observations over the rainbands of tropical cyclones. *Mon. Wea. Rev.*, **148**, 4729–4745, https://doi.org/10.1175/MWR-D-19-0341.1.
Nolan, D. S., and M. T. Montgomery, 2002: Nonhydrostatic, three-dimensional perturbations to balanced, hurricane-like vortices. Part I: Linearized formulation, stability, and evolution. *J. Atmos. Sci.*, **59**, 2989–3020, https://doi.org/10.1175/1520-0469(2002)059<2989:NTDPTB>2.0.CO;2.
Nolan, D. S., and L. D. Grasso, 2003: Nonhydrostatic, three-dimensional perturbations to balanced, hurricane-like vortices. Part II: Symmetric response and nonlinear simulations. *J. Atmos. Sci.*, **60**, 2717–2745, https://doi.org/10.1175/1520-0469(2003)060<2717:NTPTBH>2.0.CO;2.
Peng, K., R. Rotunno, and G. H. Bryan, 2018: Evaluation of a time-dependent model for the intensification of tropical cyclones. *J. Atmos. Sci.*, **75**, 2125–2138, https://doi.org/10.1175/JAS-D-17-0382.1.
Peng, K., R. Rotunno, G. H. Bryan, and J. Fang, 2019: Evolution of an axisymmetric tropical cyclone before reaching slantwise moist neutrality. *J. Atmos. Sci.*, **76**, 1865–1884, https://doi.org/10.1175/JAS-D-18-0264.1.
Pu, Z. X., and S. A. Braun, 2001: Evaluation of bogus vortex techniques with four-dimensional variational data assimilation. *Mon. Wea. Rev.*, **129**, 2023–2039, https://doi.org/10.1175/1520-0493(2001)129<2023:EOBVTW>2.0.CO;2.
Pu, Z. X., X. L. Li, and J. Z. Sun, 2009: Impact of airborne Doppler radar data assimilation on the numerical simulation of intensity changes of Hurricane Dennis near a landfall. *J. Atmos. Sci.*, **66**, 3351–3365, https://doi.org/10.1175/2009JAS3121.1.
Qiu, X., and Z.-M. Tan, 2013: The roles of asymmetric inflow forcing induced by outer rainbands in tropical cyclone secondary eyewall formation. *J. Atmos. Sci.*, **70**, 953–974, https://doi.org/10.1175/JAS-D-12-084.1.
Ren, S. J., L. L. Lei, Z.-M. Tan, and Y. Zhang, 2019: Multivariate ensemble sensitivity analysis for super typhoon Haiyan (2013). *Mon. Wea. Rev.*, **147**, 3467–3480, https://doi.org/10.1175/MWR-D-19-0074.1.
Riehl, H., 1950: A model of hurricane formation. *J. Appl. Phys.*, **21**, 917–925, https://doi.org/10.1063/1.1699784.
Riemer, M., and S. C. Jones, 2010: The downstream impact of tropical cyclones on a developing baroclinic wave in idealized scenarios of extratropical transition. *Quart. J. Roy. Meteor. Soc.*, **136**, 617–637, https://doi.org/10.1002/qj.605.
Schecter, D. A., M. T. Montgomery and P. D. Reasor, 2002: A theory for the vertical alignment of a quasigeostrophic vortex. *J. Atmos. Sci.*, **59**, 150–168, https://doi.org/10.1175/1520-0469(2002)059<0150:ATFTVA>2.0.CO;2.
Schubert, W. H., M. T. Montgomery, R. K. Taft, T. A. Guinn, S. R. Fulton, J. P. Kossin, and J. P. Edwards, 1999: Polygonal eyewalls, asymmetric eye contraction, and potential vorticity mixing in hurricanes. *J. Atmos. Sci.*, **56**, 1197–1223, https://doi.org/10.1175/1520-0469(1999)056<1197:PEAECA>2.0.CO;2.
Smith, R. K., 2003: A simple model of the hurricane boundary layer. *Quart. J. Roy. Meteor. Soc.*, **129**, 1007–1027, https://doi.org/10.1256/qj.01.197.
Sobel, A. H., A. A. Wing, S. J. Camargo, C. M. Patricola, G. A. Vecchi, C.-Y. Lee, and M. K. Tippett, 2021: Tropical cyclone frequency. *Earth's Future*, **9**(12), e2021EF002275, https://doi.org/10.1029/2021EF002275.
Sun, L. X., X. D. Tang, X. Y. Zhuge, Z.-M. Tan, and J. Fang, 2021: Diurnal variations of overshooting tops in typhoons detected by Himawari-8 satellite. *Geophys. Res. Lett.*, **48**, e2021GL095565, https://doi.org/10.1029/2021GL095565.
Tang, B., and K. Emanuel, 2010: Midlevel ventilation's constraint on tropical cyclone intensity. *J. Atmos. Sci.*, **67**, 1817–1830, https://doi.org/10.1175/2010JAS3318.1.
Tang, X. D., and F. Q. Zhang, 2016: Impacts of the diurnal radiation cycle on the formation, intensity, and structure of Hurricane Edouard (2014). *J. Atmos. Sci.*, **73**, 2871–2892, https://doi.org/10.1175/JAS-D-15-0283.1.
Tang, X. D., Q. C. Cai, J. Fang, and Z.-M Tan, 2019a: Land–sea contrast in the diurnal variation of precipitation from landfalling tropical cyclones. *J. Geophys. Res.: Atmos.*, **124**, 12 010–12 021, https://doi.org/10.1029/2019JD031454.
Tang, X. D., Z.-M. Tan, J. Fang, E. B. Munsell, and F. Q. Zhang, 2019b: Impact of the diurnal radiation contrast on the contraction of radius of maximum wind during intensification of Hurricane Edouard (2014). *J. Atmos. Sci.*, **76**, 421–432, https://doi.org/10.1175/JAS-D-18-0131.1.
Torn, R. D., 2010: Performance of a mesoscale ensemble Kalman Filter (EnKF) during the NOAA high-resolution hurricane test. *Mon. Wea. Rev.*, **138**, 4375–4392, https://doi.org/10.1175/2010MWR3361.1.
Ueno, M., 1995: A study on the impact of asymmetric components around tropical cyclone center on the accuracy of bogus data and the track forecast. *Meteorol. Atmos. Phys.*, **56**, 125–134, https://doi.org/10.1007/BF01022525.
Van Nguyen, H., and Y. L. Chen, 2011: High-resolution initialization and simulations of Typhoon Morakot (2009). *Mon. Wea. Rev.*, **139**, 1463–1491, https://doi.org/10.1175/2011MWR3505.1.

Wang, C., L. L. Lei, Z.-M. Tan, and K. K. Chu, 2020: Adaptive localization for Tropical cyclones with satellite radiances in an ensemble Kalman filter. *Frontiers in Earth Science*, **8**, 39, https://doi.org/10.3389/feart.2020.00039.

Wang, H., and Y. Q. Wang, 2021: A numerical study of Typhoon Megi (2010). Part II: Eyewall evolution crossing the Luzon Island. *Mon. Wea. Rev.*, **149**, 375–394, https://doi.org/10.1175/MWR-D-19-0380.1.

Wang, H., Y. Q. Wang, J. Xu, and Y. H. Duan, 2019a: The axisymmetric and asymmetric aspects of the secondary eyewall formation in a numerically simulated tropical cyclone under idealized conditions on an *f* Plane. *J. Atmos. Sci.*, **76**, 357–378, https://doi.org/10.1175/JAS-D-18-0130.1.

Wang, H., Y. Q. Wang, J. Xu, and Y. H. Duan, 2019b: Evolution of the warm-core structure during the eyewall replacement cycle in a numerically simulated tropical cyclone. *J. Atmos. Sci.*, **76**, 2559–2573, https://doi.org/10.1175/JAS-D-19-0017.1.

Wang, Q., Y. L. Xu, N. Wei, S. Wang, and H. Hu, 2019c: Forecast and service performance on rapidly intensification process of typhoons Rammasun (2014) and Hato (2017). *Tropical Cyclone Research and Review*, **8**(1), 18–26, https://doi.org/10.1016/j.tcrr.2019.07.002.

Wang, Y.-F., and Z.-M. Tan, 2020: Outer rainbands-driven secondary eyewall formation of tropical cyclones. *J. Atmos. Sci.*, **77**, 2217–2236, https://doi.org/10.1175/JAS-D-19-0304.1.

Wang, Y. Q., 2009: How do outer spiral rainbands affect tropical cyclone structure and intensity. *J. Atmos. Sci.*, **66**, 1250–1273, https://doi.org/10.1175/2008JAS2737.1.

Wang, Y. Q., and G. J. Holland, 1996: Tropical cyclone motion and evolution in vertical shear. *J. Atmos. Sci.*, **53**, 3313–3332, https://doi.org/10.1175/1520-0469(1996)053<3313:TCMAEI>2.0.CO;2.

Weissmann, M., and Coauthors, 2011: The influence of assimilating dropsonde data on typhoon track and midlatitude forecasts. *Mon. Wea. Rev.*, **139**, 908–920, https://doi.org/10.1175/2010MWR3377.1.

Wu, C.-C., K.-H. Chou, P.-H. Lin, S. D. Aberson, M. S. Peng, and T. Nakazawa, 2007: The impact of dropwindsonde data on typhoon track forecasts in DOTSTAR. *Wea. Forecasting*, **22**, 1157–1176, https://doi.org/10.1175/2007WAF2006062.1.

Wu, S. L., and J. Fang, 2019: The evolution and role of midtropospheric cyclonic vortex in the formation of Super Typhoon Nepartak (2016). *J. Geos. Res.: Atmos.*, **124**, 9277–9298, https://doi.org/10.1029/2019JD030631.

Wu, T.-C., M. Zupanski, L. D. Grasso, C. D. Kummerow, and S.-A. Boukabara, 2019: All-sky radiance assimilation of ATMS in HWRF: A demonstration study. *Mon. Wea. Rev.*, **147**, 85–106, https://doi.org/10.1175/MWR-D-17-0337.1.

Xiao, J., Z.-M. Tan, and K. C. Chow, 2019: Structure and formation of convection of secondary rainbands in a simulated typhoon Jangmi (2008). *Meteorol. Atmos. Phys.*, **131**, 713–737, https://doi.org/10.1007/s00703-018-0599-0.

Xiao, Q. N., L. Q. Chen, and X. Y. Zhang, 2009: Evaluations of BDA scheme using the Advanced Research WRF (ARW) model. *J. Appl. Meteorol. Climatol.*, **48**, 680–689, https://doi.org/10.1175/2008JAMC1994.1.

Xiao, Q. N., Y.-H. Kuo, Y. Zhang, D. M. Barker, and D.-J. Won, 2006: A tropical cyclone bogus data assimilation scheme in the MM5 3D-Var system and numerical experiments with Typhoon Rusa (2002) near landfall. *J. Meteor. Soc. Japan. Ser. II*, **84**, 671–689, https://doi.org/10.2151/jmsj.84.671.

Xin, J. J., H. Yu, and P. Y. Chen, 2021: Evaluation of tropical cyclone intensity forecasts from five global ensemble prediction systems during 2015-2019,. *Journal of Tropical Meteorology*, **27**(3), 218–231, https://doi.org/10.46267/j.1006-8775.2021.020.

Xu, H.-X., and Y. Q. Wang, 2021: Sensitivity of fine-scale structure in tropical cyclone boundary layer to model horizontal resolution at sub-kilometer grid spacing. *Frontiers in Earth Science*, **9**, 707274, https://doi.org/10.3389/feart.2021.707274.

Yang, B. L., and Z.-M. Tan, 2020: Interactive radiation accelerates the intensification of the midlevel vortex for tropical cyclogenesis. *J. Atmos. Sci.*, **77**, 4051–4065, https://doi.org/10.1175/JAS-D-20-0094.1.

Zhang, F. Q., M. Minamide, and E. E. Clothiaux, 2016: Potential impacts of assimilating all-sky infrared satellite radiances from GOES-R on convection-permitting analysis and prediction of tropical cyclones. *Geophys. Res. Lett.*, **43**, 2954–2963, https://doi.org/10.1002/2016GL068468.

Zhang, F. Q., Y. H. Weng, J. A. Sippel, Z. Y. Meng, and C. H. Bishop, 2009: Cloud-resolving hurricane initialization and prediction through assimilation of Doppler radar observations with an ensemble Kalman filter. *Mon. Wea. Rev.*, **137**, 2105–2125, https://doi.org/10.1175/2009MWR2645.1.

Zhang, J. A., E. A. Kalina, M. K. Biswas, R. F. Rogers, P. Zhu, and F. D. Marks, 2020: A review and evaluation of planetary boundary layer parameterizations in Hurricane Weather Research and Forecasting Model using idealized simulations and observations. *Atmosphere*, **11**, 1091, https://doi.org/10.3390/atmos11101091.

Zhang, Z., Y. Q. Wang, W.-M. Zhang, and J. Xu, 2019: Coastal ocean response and its feedback to Typhoon Hato (2017) over the South China Sea: A numerical study. *J. Geophys. Res.: Atmos.*, **124**(24), 13 731–13 749, https:/doi.org/10.1029/2019JD031377. https://doi.org/10.1029/2019JD031377.

Zhao, J. W., R.-F. Zhan, and Y. Q. Wang, 2018: Global warming hiatus contributed to the increased occurrence of intense tropical cyclones in the coastal regions along East Asia. *Scientific Reports*, **8**, 6023, https://doi.org/10.1038/s41598-018-24402-2.

Zhou, F. F., and Z. Toth, 2020: On the prospects for improved tropical cyclone track forecasts. *Bull. Amer. Meteor. Soc.*, **101**, E2058–E2077, https://doi.org/10.1175/BAMS-D-19-0166.1.

Zhou, F. F., W. S. Duan, H. Zhang, and M. Yamaguchi, 2018: Possible sources of forecast errors generated by the Global/Regional Assimilation and Prediction System for landfalling tropical cyclones. Part II: Model uncertainty. *Adv. Atmos. Sci.*, **35**, 1277–1290, https://doi.org/10.1007/s00376-018-7095-9.

Zhou, Y. C., J. W. Zhao, R. F. Zhan, P. Y. Chen, Z. W. Wu, and L. Wang, 2021: A Logistic-growth-equation-based Intensity Prediction Scheme for Western North Pacific Tropical Cyclones. *Adv. Atmos. Sci.*, **38**(10), 1750–1762, https://doi.org/10.1007/s00376-021-0435-1.

Zhu, Y. Q., G. Gayno, R. J. Purser, X. J. Su, and R. H. Yang, 2019: Expansion of the all-sky radiance assimilation to ATMS at NCEP.

Mon. Wea. Rev., **147**(7), 2603–2620, https://doi.org/10.1175/MWR-D-18-0228.1.

Zhuge, X., X. Zou, F. Weng, and M. Sun, 2018: Dependence of simulation biases of AHI surface-sensitive channels on land surface emissivity over China. *J. Atmos. Oceanic Technol.*, **35**(6), 1283–1298, https://doi.org/10.1175/JTECH-D-17-0152.1.

Zhuge, X. Y., X. L. Zou, and Y. Wang, 2021a: Determining AHI cloud-top phase and intercomparisons with MODIS products over North Pacific. *IEEE Trans. Geosci. Remote Sens.*, **59**(1), 436–448, https://doi.org/10.1109/TGRS.2020.2990955.

Zhuge, X. Y., X. L. Zou, and Y. Wang, 2021b: AHI-derived daytime cloud optical/microphysical properties and their evaluations with the collection-6.1 MOD06 Product. *IEEE Trans. Geosci. Remote Sens.*, **59**, 6431–6450, https://doi.org/10.1109/TGRS.2020.3027017.

Zhuo, J.-Y., and Z.-M. Tan, 2021: Physics-augmented deep learning to improve tropical cyclone intensity and size estimation from satellite imagery. *Mon. Wea. Rev.*, **149**, 2097–2113, https://doi.org/10.1175/MWR-D-20-0333.1.

Zou, X. L., and Q. N. Xiao, 2000: Studies on the initialization and simulation of a mature hurricane using a variational bogus data assimilation scheme. *J. Atmos. Sci.*, **57**, 836–860, https://doi.org/10.1175/1520-0469(2000)057<0836:SOTIAS>2.0.CO;2.